EIJEST

PARAMETRIC STUDY OF AIR COOLING PROCESS VIA WATER COOLED BUNDLE OF WING-SHAPED TUBES*

Sayed Ahmed E. Sayed Ahmed, Osama M. Mesalhy, Tarek M. Khass, Abdulrahman H. Hassan**

Mechanical Power Eng. Dept., Faculty of Engineering, Zagazig University, Egypt

ABSTRACT

This study presents an experimental and numerical study of flow and heat transfer characteristics of a cross flow heat exchanger employing staggered wing shaped tubes with zero angle of attack. Hot air was forced to flow over the external surface of the tubes and exchange heat with the cold water flowing inside. The water side Re_w was varied from 5×10^2 to 1×10^3 and the air side Re_a was varied from 1.85×10^3 to 9.7×10^3. Correlations of Nu_a, St_a, P_{dc}, as well as the heat transfer per unit pumping power ε against Re_a and design parameters are presented. Comparing with other different shapes from literature it is concluded that enhancement in the heat transfer of 34 % and reduction in the pressure drop of 37 % are achieved by utilizing the wing-shaped tubes as relative to the circular ones. The heat transfer coefficient, effectiveness, and efficiency index for bundles of circular, elliptical and wing-shaped tubes were compared. The results indicate that, the bundle of wing-shaped tubes has better performance over other bundles for similar parameters and conditions.

KEY WORDS: Bundle of wing-shaped tubes, Heat Exchanger, Cross-flow cooling, and CFD**.**

ÉTUDE PARAMETRIQUE DU PROCESSUS DE REFROIDISSEMENT AIR REFROIDI PAR EAU VIA BUNDLE DE L'AILE EN FORME DE TUBES

RÉSUMÉ

Cette étude présente une étude expérimentale et numérique de l'écoulement et les caractéristiques de transfert de chaleur d'un échangeur de chaleur à plaques en quinconce employant des ailes en forme de tubes avec zéro angle d'attaque. L'air chaud est forcé de s'écouler sur la surface extérieure des tubes d'échange de chaleur et à l'eau froide circulant à l'intérieur. Le Rew côté de l'eau a varié de 5×102 à 1×103 and côté air Rea a varié de $1,85 \times 103$ à $9,7 \times 103$. Les corrélations de Nua, Sta, Pdc, ainsi que le transfert de chaleur par unité de puissance de pompage ε contre Rea et les paramètres de conception sont présentés. Comparaison avec d'autres formes de la littérature, il est conclu que l'amélioration du transfert de chaleur de 34% et une réduction de la perte de charge de 37% sont obtenus en utilisant des tubes en forme d'ailes en tant que rapport à ceux circulaires. L'indice de coefficient de transfert de chaleur, l'efficacité et l'efficience des faisceaux de tubes circulaires, elliptiques et en forme d'aile ont été comparés. Les résultats indiquent que, le faisceau de tubes en forme d'aile a de meilleures performances sur les autres bundles pour les paramètres et des conditions similaires.

MOTS CLÉS: Ensemble de l'aile en forme de tubes, échangeurs de chaleur, refroidissement à flux transversal et CFD.

Sayed Ahmed, Mesalhy, Khass, Hassan

1. INTRODUCTION

The increase in energy demand in all sectors of the human society requires an increasingly more intelligent use of available energy. Many industrial applications require the use of heat exchangers with different tubes' arrangements, either finned or non-finned, as in air conditioning systems, refrigeration, heaters, radiators, etc. Such devices have to be compact, lightweight and high performance. A review of the available literature has shown that the thermal and hydraulic performance of heat exchangers relay upon many parameters. Such parameters include: tube shape, arrangement of tubes, orientations of tubes etc.

There are numerous studies which take into consideration the effect of tube shape and bundle geometry on the performance of heat exchangers. For example, Zukauskas and Ulinskas [1] suggested correlations for heat transfer and pressure drop for in-line and staggered banks of circular tubes. Their study covered the range of $1 < \text{Re} < 2 \times 10^{6}$, $0.7 < \text{Pr} < 500$, as well as a wide range of relative transverse and longitudinal pitches. They suggested an efficiency factor for the evaluation of efficiency of heat transfer surfaces in further improvement of heat exchangers constructions. Fluid flow and heat transfer characteristics in semi-circular tube placed in cross flow have been numerically and experimentally investigated by Nada et al. [2] for a wide range of Re. They mentioned that the semi-circular tube has higher Nu than the circular one. Comparisons of circular and elliptical tubes as the essential elements of heat exchangers have been reported in several studies. For example, Brauer [3] reported 18 % of relative reduction in the pressure drop for elliptical compared to circular. Horvat et al. [4] made a numerical research to study the transient heat transfer and fluid flow for circular, elliptical, and wing shaped tubes with the same cross section. Comparing the three types of tubes, they reported that the values of average drag coefficient and Stanton number are lower for the ellipsoidal and the wing-shaped tubes than for the cylindrical tubes.

The axis ratio of the tube is an important parameter which has been investigated deeply in many studies such as Badr [5] in his study of forced convection from an elliptical tube located in cross flow of air has examined the effect of the axis ratio on heat transfer. The investigation included four axis ratios, 0.4, 0.5, 0.7, and 0.9, for Re in the range from 200 to 500, the results showed that the 0.4 axis ratio provided the highest heat transfer rate.

Also, tube spacing and blockage ratio have a crucial impact on the heat transfer and pressure drop through the heat exchanger. This impact has been studied extensively by Wilson et al. [6]. They have theoretically studied heat transfer and pressure drop characteristics of single row of circular tubes in cross air flow. The Re ranged from 500 to 100000. They examined the tube spacing effect in the form of traverse- spacing to diameter ratio. This spacing ratio was varied from 1.3 to 5. They revealed that the maximum heat transfer coefficient and the minimum pressure loss are obtained at smallest traverse-spacing to diameter ratio (1.3). On the other hand, Nishiyama et al. [7] conducted an experimental study of flow pattern and heat transfer characteristics around four cylinders of elliptical cross sections. The cylinders have a major axis of 50 mm and a minor to major axis ratio of 0.5. Considering the major axis as the characteristic length, Re was varied from 15000 to 70000. The cylinders spacing in the dimensionless form of center- to-center distance to major axis ratio was ranged from 1.25 to 4. The results indicated that to achieve high heat transfer coefficient, the cylinders are to be spaced as close to each other as possible.

Flow angle of attack is another important parameter which influences significantly the overall performance of heat exchangers. Ibrahim and Gomma [8] have performed experimental and numerical studies of the turbulent flow over bundle of elliptical tubes. Their investigation covers a range of Re from 5600 to 40000 with four axis ratios considered (0.25, 0.33, 0.5 and 1) and the flow angle of attack was varied from 0° to 150°. Their results show that the thermal performance under a fixed pumping power was best at 0° and worst at 90° flow angles of attack. Ibrahim et al.[9], conducted an experimental investigation of

the performance of a bundle of semi-circular tubes. The air flow Reynolds number ranged from 2×10^4 to 16.5×10^4, the angle of attack was varied from 0° to 270° and the relative longitudinal pitch S_L/d from 1.35 to 2.69, while the relative transverse pitch was kept at $S_t/d = 1.35$. They conclude that the highest and the lowest values of Nu and effectiveness occur at 270° and 0° angle of attack for all values of S_L/d, respectively.

An experimental study of air cooling and dehumidification around a bank of in-line elliptical tubes in cross flow heat exchanger was conducted by Ibrahiem et al. [10]. They conclude that; (a): the Colburn j-factor increases with the the angle of attack α for constant relative transverse pitch for the given range of relative longitudinal pitch, (b): the effectiveness ε of the wet surfaces of the tested bundle increases with α.

It appears from the literature that there are only a few studies that considered wing-shaped tubes. So in the current study, the heat transfer and flow characteristics of a bundle of staggered wing-shaped tubes placed in cross flow were experimentally and numerically investigated, using air and water as standard heat transfer media.

2. EXPERIMENTAL DETAILS AND DATA COLLECTION

The experiments were conducted in an open-suction-type wind tunnel of 2780 mm length, as shown in Fig. (1). The tunnel is capable of producing an air velocity up to 7.3 m/s. The plexiglas test section of 305 mm×305 mm, and 780 mm long is mounted in the middle of the wind tunnel. The cross-sectional dimensions of wing-shaped tube, drawn from 1 mm thick, 22.44 mm outer diameter circular copper tube with 305 mm long, is shown in Fig. (2a). The tested tube bundle, shown in Fig. (2b), consist of 22 wing-shaped tubes. They are staggerly arranged at zero angle of attack and distributed through three successive rows. Longitudinal and transverse tube-pitches of 37 mm were kept constant. Two half dummy tubes were placed at each side of the bundle to minimize external strays.

4 kW electrical heaters in the wind tunnel were the source for supplying heat to the inlet air. Air at 48.5±1.5°C dry bulb and 24±1.5 °C wet bulb temperature entered the test section and passed over the tube bundle. Inside the tubes cold water at 7.6±1.5 °C entered at the bottom of the bundle.

2.1 Measuring Techniques

T-type thermocouples were used to measure temperature. Water flow inlet, T_{wi} and exit, T_{we} temperatures, were measured by means of a single point measurement. Air flow inlet, T_{ai} and exit, T_{ae} average temperatures, were measured by thermocouples arranged in grids. For the inlet measurement, a grid of three thermocouples arranged uniformly across the inlet cross section was used. At the exit cross section, a grid consisting of 5 points was used to estimate the average temperature at the exit. In addition, the wet bulb temperatures at inlet and exit were measured by using alcohol thermometer with wet wick surrounded bulb. The surface temperatures of the tubes, T_s were measured by attaching 2 thermocouple probes on the outer surface of each tube of the tested bundle. The average temperature of every tube was taking to be as the average of the two probes attached to its surface. A hand-held digital thermometer with an uncertainty of $\pm$ (0.2 °C + 0.05% of reading) was used to record all the temperatures.

To measure the airflow pressure drop in the test section, four pressure taps were drilled as depicted in Fig. (3). The pressure drops (ΔP_a) were measured along pressure taps using an electrical micro-manometer of $\pm$ 0.1 mm H_2O accuracy of full scale, (manufactured by Furness controls company, model FC 001, and serial number (FN 2561).

Sufficient times were allowed to get the air stabilized to the desired temperature and the stabilization times were observed to be roughly 120–160 min. Experimental data involved the measurements of the surface temperatures of the wing-shaped tubes, air inlet and exit temperatures, water inlet and exit temperatures, and water mass flow rates corresponding to four predetermined values of mean flow air velocity in the wind tunnel.
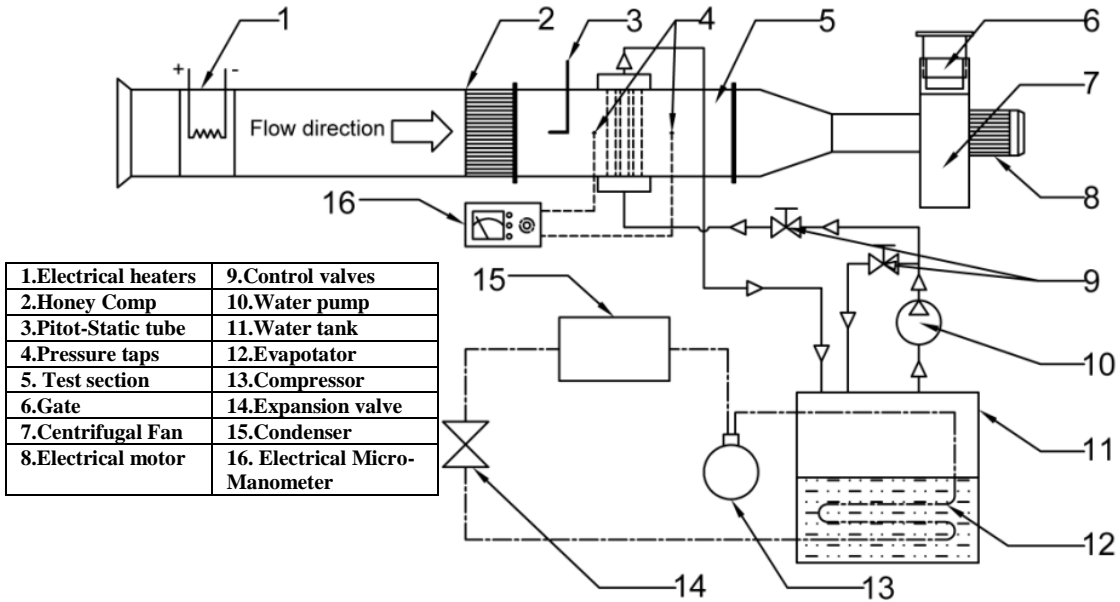
Fig. (1) Open-suction thermal wind tunnel.

1.Electrical heaters	9.Control valves
2.Honey Comp	10.Water pump
3.Pitot-Static tube	11.Water tank
4.Pressure taps	12.Evapotator
5. Test section	13.Compressor
6.Gate	14.Expansion valve
7.Centrifugal Fan	15.Condenser
8.Electrical motor	16. Electrical Micro-Manometer
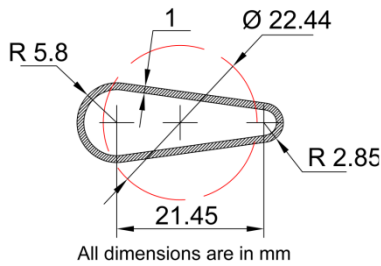
(a)
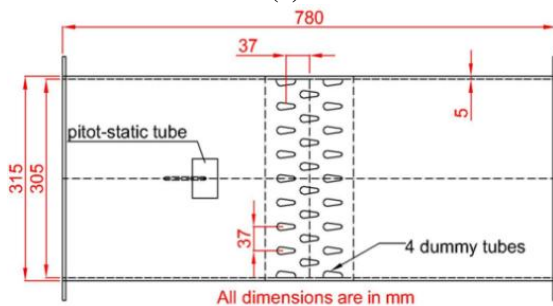
(b)

Fig.(2) (a) Wing-shaped tube cross sectional dimensions, (b) Schematic of the test section

Four different cold-water mass flow rates (m_w) of 0.205, 0.26, 0.35 and 0.43 kg/s were investigated. The water flow rates were measured at the beginning of each test using bucket stopwatch method.
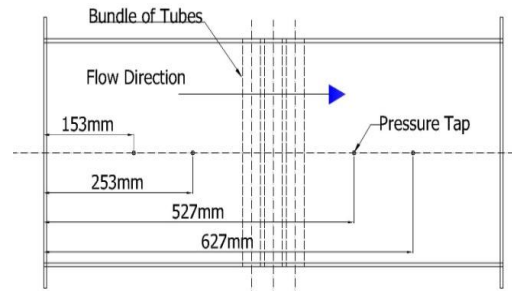
Fig. (3) Locations of the pressure taps

The mean air flow velocity (V_{ai}) was varied from 1.33 to 7 m/s, giving air side Reynolds numbers ranging from 1.85×10^3 to 9.7×10^3 for each cold-water flow rate. At the air inlet of the test section, air velocity profile was performed in the presence of the bundle of wing-shaped tubes heat exchanger. The velocity profile was observed to be uniform for the entire cross section, outside the boundary layer, with the maximum deviation of around 3% from the mean. The air velocities for subsequent experiments were measured at a single point around the center-entrance of the test section with a 3 mm Pitot static tube using the same electrical micro-manometer as used in the pressure drop measurement.

2.2 Data Reduction

Steady state flow conditions were achieved during the experiments. The fluid properties, for both air and water, were determined from tables given by Cengel [11]. If not mentioned otherwise, all the thermo physical properties for air were evaluated at film temperature, $\left(T_{af} = \dfrac{T_{ai} + T_s}{2}\right)$, while for water at bulk temperature, T_{wb}.

The present experimental study is divided into two parts: fluid flow and heat transfer studies. The essential quantities determined in the current study are as the followings:

2.2.1 Fluid flow consideration

Mean inlet air velocity can be calculated from the measured data by the standard Pitot tube through the following relationship:

$$V_{ai} = \sqrt{2g\left(\rho_w / \rho_a\right)\Delta h_{dyn}}, \quad (m/s) \qquad (1)$$

where, Δh_{dyn} is the head difference between the total and static pressure heads through Pitot tube, m H_2O, while ρ_a and ρ_w are the air and water density respectively, kg/m^3.

The pressure drop coefficient, P_{dc}, as defined below in Eq. (2), represents the ratio of the irreversible pressure drop of the moving air over the tube array to its dynamic pressure

$$P_{dc} = \frac{2\Delta p_a}{\rho_{af} \, V_{ai}^{\,2}} \qquad (2)$$

where, the pressure drop through the tube bundle, Δp_a was measured by the electrical micro-manometer via pressure taps, and ρ_{af} is the air film density.

2.2.2 Heat transfer consideration

The water side heat gain rate was calculated as:

$$Q_w = m_w c_{p_w} (T_{we} - T_{wi}), \quad (W) \qquad (3)$$

While, the air side heat transfer rate was calculated as:

$$Q_a = m_a c_{p_{af}} (T_{ai} - T_{ae}), \quad (W) \qquad (4)$$

where, m_w and m_a are the mass flow rates for water and air, kg/s, respectively. T_{wi}, T_{we}, T_{ai}, T_{ae} are the water and air inlet and exit temperatures, respectively.

The average air and water heat transfer rate, Q, is used to determine the average heat transfer coefficient for air.

$$Q = \frac{Q_a + Q_w}{2}, \quad (W) \qquad (5)$$

the air side average heat transfer coefficient, h_a was determined as:

$$h_a = \frac{Q}{A_{s_0} \Delta T_{ln}}, \quad (W/m^2.K) \qquad (6)$$

Where, A_{so}, is the total outer surface area for the tubes and, ΔT_{ln} is the logarithmic mean temperature difference.

The Reynolds number, Re_a is given by:

$$Re_a = \frac{\rho_{af} V_{ai} D_{eq}}{\mu_{af}} \qquad (7)$$

Based on h_a, Re_a, and the equivalent diameter D_{eq} which is used as the characteristic, Nusselt number Nu_a is defined as:

$$Nu_a = \frac{h_a D_{eq}}{k_{af}} \qquad (8)$$

where, k_{af} is air thermal conductivity, W/m.K.

2.3 Measurement Uncertainties

The experimental error analysis indicates the implication of error of the measured parameters on the uncertainty of the results. A detailed analysis of the various experimental uncertainties is carried out using the differential approximation method for error analysis [12]. The maximum errors in measuring parameters are: temperature $\pm1.33\%$, pressure drop across the heat exchanger and dynamic pressure at inlet $\pm4.5\%$, and 3%, respectively. However, the maximum uncertainties of the results that have been obtained from the measured parameters for air flow velocity(V_{ai}), water flow velocity(V_{wi}), heat transfer coefficient(h_a), Nusselt number(Nu_a), pressure drop coefficient(P_{dc})and heat transfer per unit pumping power(ε) are $\pm1.514\%$, $\pm1.5\%$, $\pm2.18\%$, $\pm2.18\%$, $\pm5.5\%$, $\pm4.6\%$, respectively.

3. NUMERICAL INVESTIGATION

3.1 Problem Description and Boundary Conditions

Since, the tube length is much greater than its equivalent diameter, the flow across the tube bundle is considered two-dimensional. The geometry of the numerical model includes entrance section, tube bundle section, and exit section beside the boundary conditions, are shown in Fig.(4). The numerical solution is carried out by solving the governing equations of mass, momentum and energy under the following assumptions; the flow is incompressible, steady and turbulent, fluid properties are constant, the effect of buoyancy force and radiation are neglected. Based on the aforementioned assumption, Fluent [13]:

$$\frac{\partial}{\partial x_i} = 0.0 \tag{9}$$

$$\frac{\partial}{\partial x_j}(\rho V_i V_j) = -\frac{\partial p}{\partial x_i} + \frac{\partial \tau_{ij}}{\partial x_j} \tag{10}$$

$$\frac{\partial}{\partial x_i}[V_i(\rho E + p)] = \frac{\partial}{\partial x_i}\left(k\,\frac{\partial T}{\partial x_i}\right) \tag{11}$$

where, i: is a tensor indicating 1and2, τ_{ij} is the viscous stress tensor, and k is the fluid effective thermal conductivity.
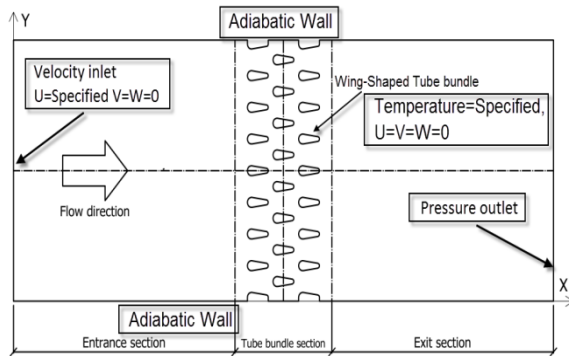
Fig.(4) Boundary conditions for the numerical domain

Commercial CFD software FLUENT 6.3.26 is used to solve the governing equations. RNG κ–ε turbulent model is utilized to solve the complicated turbulent thermal flow field with Enhanced Wall Function approach in the near-wall regions to fit the wall boundary conditions, Fluent [13].

3.2 Mesh Generation and Discretization

The geometry and mesh of the computational model that described in the previous section were generated separately using GAMBIT 2.4.6. Quad/Map, Tri/Pave and boundary layer meshing scheme was used in the present study with refining the mesh near walls and beside sharp edges.

Fig. (5) shows the configuration of the computational domain mesh. To test the dependence of the numerical results on the grid density, calculations were carried out with different mesh densities in the x and y directions. As recommended by Fluent [13], the first grid points adjacent to the walls were kept at y^+ values between 1 and 5. The grid sensitivity analysis was carried out mainly to obtain grid independent temperature distributions. The computational results of the mean heat transfer coefficient through the tube bundle varied to give about 6.8 % decrease when the number of grids increased from 69,312 to 70,922. When the grid size increased from 70,922 to 132,010 only 2.43% increase in heat transfer coefficient is obtained, further increasing in grid size up to 339,970 decreased the variation to only 0.4% as shown in Fig. 6. It is clear that the effect of grid size on the computed result diminishes for grids of 132,010 nodes.

A finite volume discretization method using second order upwind schema for momentum, turbulent kinetic energy, and turbulent dissipation rate was applied, besides using SIMPLE-based solution algorithm of the velocity–pressure coupling with a segregated solver.

The solution was considered converged when the scaled residual of the energy equation reaches 10^{-7} and the scaled residuals of other equations reach 10^{-4}.

(a)

(b)
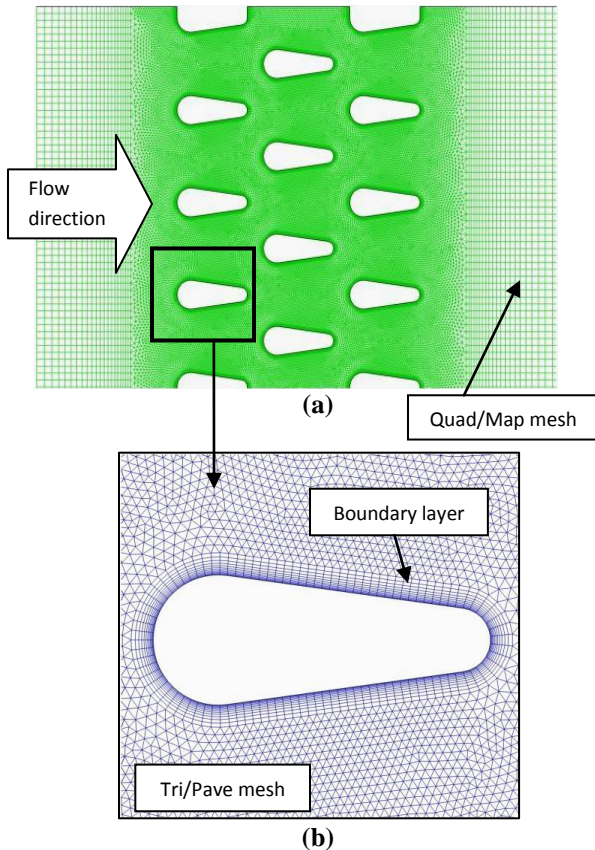
Fig. (5) (a) Mesh configuration for the domain of tube bundle, (b) Mesh details around the wing-shaped tube.
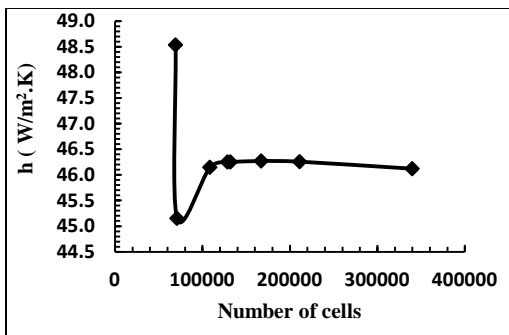
Fig.(6) Grid dependence test

4. RESULTS AND DISCUSSION

4.1 Flow Characteristics over the Bundle of Wing-Shaped Tubes:

The flow path lines and velocity contours across the tube bundle with the angle of attack $\alpha=0$, are illustrated in Fig. (7) and (8), respectively.

As shown in this Fig.(7), at low Re_a there are small eddies at lateral surfaces and at the

rear portion of the tube, which occur when the boundary layer develops against an adverse pressure gradient that makes the speed of the boundary layer relative to the object falls almost to zero. The fluid flow becomes detached from the surface of the object, and instead takes the forms of eddies and vortices. In aerodynamics, flow separation can often result in increased drag, particularly pressure drag which is caused by the pressure differential between the front and rear surfaces of the object as it travels through the fluid.

As the Re_a is increased the eddies and vortices at lateral surfaces disappeared and only the eddies at the rear portion are existed. This behavior occurred because the increasing in air velocity generates rapid flow in the transverse direction, which enable the boundary layer to travel further along the surface before separation occurs resulting, only, in a narrower wake at the rear portion of the tube.

$Re_a = 1.85 \times 10^3$

$Re_a = 9.7 \times 10^3$
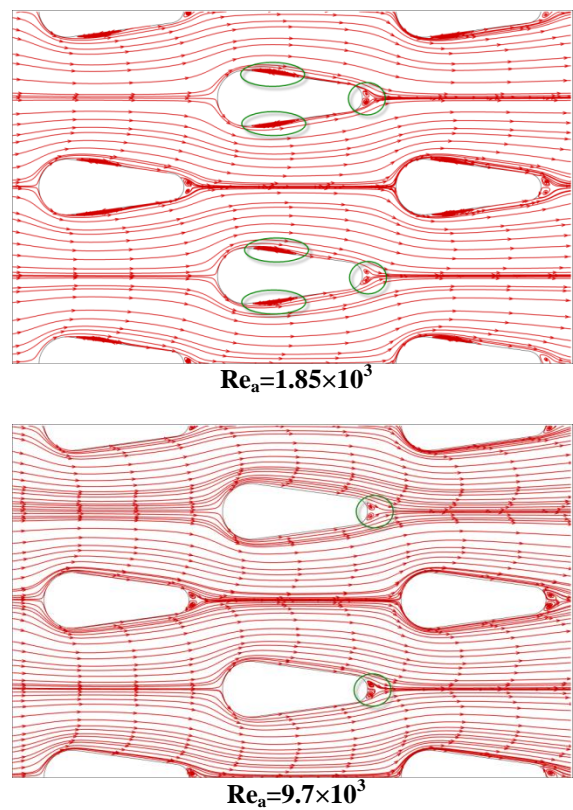
Fig.(7) Flow path lines(streamlines)

Velocity contours are depicted in Fig.(8), the airflow is strongly accelerated in the passages between two tubes with maximum velocities

lateral to the deeper rows of the bundle of wing-shaped tubes. This acceleration tends to increase the heat transferred from air to the tubes surface.

Re$_a$=1.85×10^3
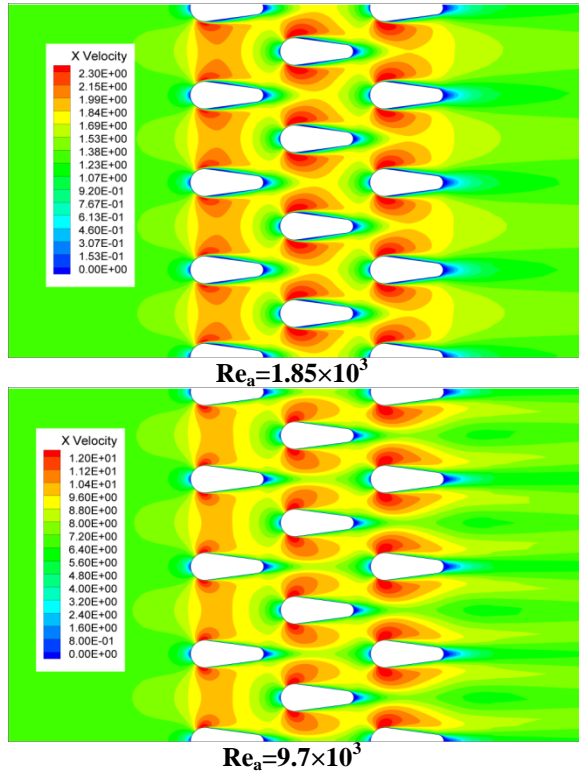
Re$_a$=9.7×10^3
Fig. (8) Velocity contours at two Re values

Comparing Fig.(7), for the current bundle, with Fig.(9) for circular ones. It can be seen that the air flow separation at the circular tubes surface is started at an earlier stage than that of the wing-shaped tubes with α=0.
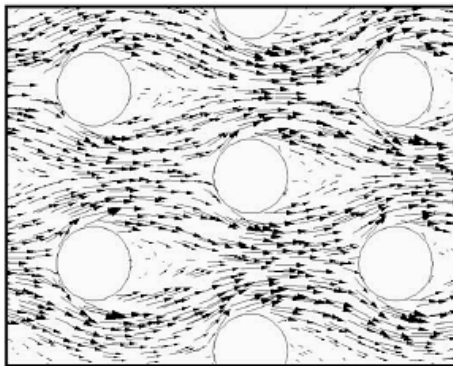
Fig. (9) Velocity vectors for circular tubes at Re ≈ 10000, Ibrahim and Gomma [8]

4.2 Heat Transfer Characteristics over the Bundle of Wing-Shaped Tubes
Temperature contours are depicted in Fig. (10) at different Re$_a$. For, comparatively, low

Re$_a$, we can notice that the thermal boundary layer is thicker than that for high Re$_a$. This is attributed to the lower inlet velocity and the separation of the flow over the tube surface. Increasing Re$_a$ will make the thermal boundary thinner. Consequently, it is expected that the heat transfer coefficient h$_a$, and Nu$_a$ will increase with Re$_a$.

Re$_a$=1.85×10^3
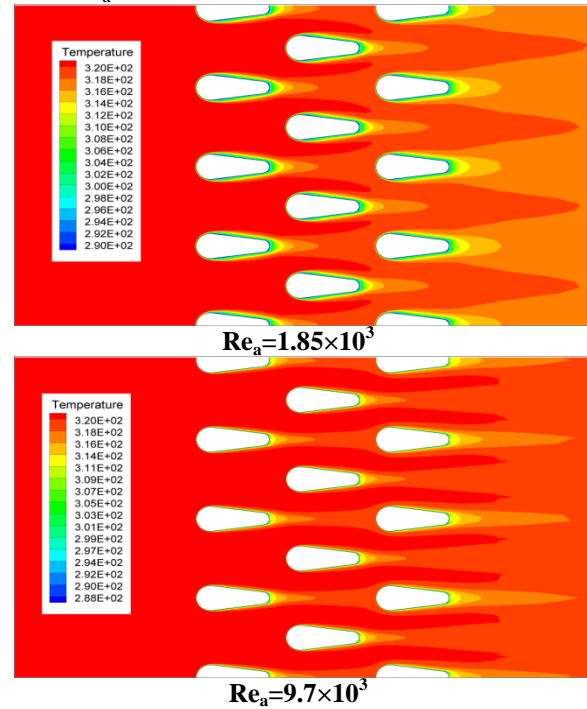
Re$_a$=9.7×10^3
Fig. (10) Temperature contours for two Re values

4.2.1 Effect of Reynolds number on heat transfer
The variations of the air flow Nu$_a$ with Re$_a$ for the bundle of wing-shaped tubes is shown below in Fig. (11). Air was forced to flow over the bundle at six different Re$_a$ ranging from 1.85×10^3 to 9.7×10^3, and exchange heat with water at different Re$_w$, varying from 5×10^2 to 1×10^3.

The results show that for given water flow rate, increasing Re$_a$ results in an increase in Nu$_a$ in a power law form for the bundle of wing-shaped tubes for the entire range of Re$_a$ considered. From the obtained data, it is obvious that the water flow rate has approximately a little effect on the heat transfer results for the air flow. The Nu$_a$ values were nearly unchanged for the entire flow range investigated. The average heat transfer for the air flow was rather influenced by the air flow rate. This is attributed

to the high thermal resistance at the air side which is always greater than that of the water side.

From the results shown in Fig. (11), average heat transfer correlation is obtained in term of Nu_a with its dependency on Re_a as following:

$$Nu_a = 0.94 \, Re_a^{0.483}, \quad R^2 = 0.95$$
$$1.85 \times 10^3 \leq Re_a \leq 9.7 \times 10^3 \tag{12}$$
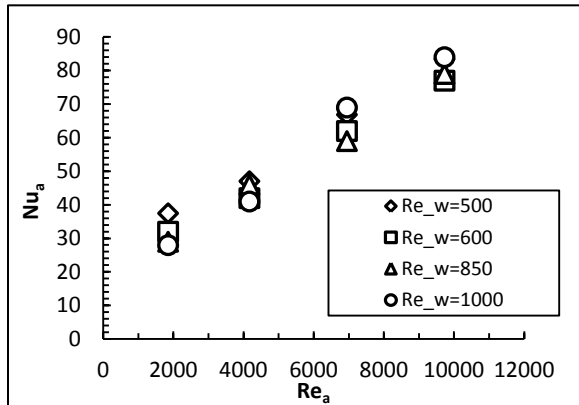
Fig. (11) Nu_a as a function of Re_a for different Re_w (Experimental)

Fig. (12), portrays overall Nu_a variation with respect to Re_a for the tube bundle (both numerical and experimental). As expected, the results show that at low Re_a, the thermal resistance of the air is high. Thus, low Nu_a was obtained. The results illustrate that the Nu_a constantly increases as Re_a increases.
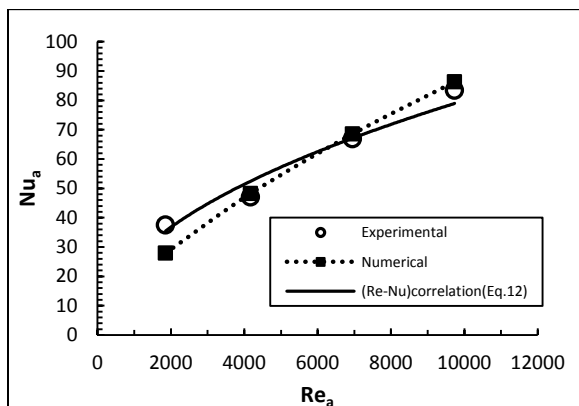
Fig. (12) Effect of Re_a on average Nu_a for present study

4.3 Air Flow Pressure Drop through the Bundle of Wing-Shaped Tubes

The pressure drop features are investigated for air flow Re_a ranging from 1.85×10^3 to 9.7×10^3 for the current tube bundle. To correlate the pressure drop coefficient with Re_a, the air flow Re_a is varied in four steps with different Re_w. The experimental data obtained for the tube bundle is combined in one overall correlation. Eq. (13) represents the correlation for the bundle of wing-shaped tubes:

$$P_{dc} = 6.731 \, Re_a^{-0.238}, \quad R^2 = 0.97$$
$$1.85 \times 10^3 \leq Re_a \leq 9.7 \times 10^3 \tag{13}$$

Fig. (13) shows the air flow pressure drop coefficient for both numerical and experimental results for the tested bundle, the average estimated error between them doesn't exceed 14%. As seen, for the range of Re_a covered in the present study, the pressure drop coefficient reached a maximum value at the Re_a value of 1.85×10^3. After that, it begun to decrease steadily as Re_a increases until reached its minimum value at a Re_a of 9.7×10^3. This is due to the fact that the overall drag consists of two combined parts. One part represents the pressure drag and another one accounts for to the friction drag. At lower Re_a, the friction drag is more important than the pressure drag leading to higher pressure drop. In the contrary, at higher Re_a, the pressure drag is predominant.
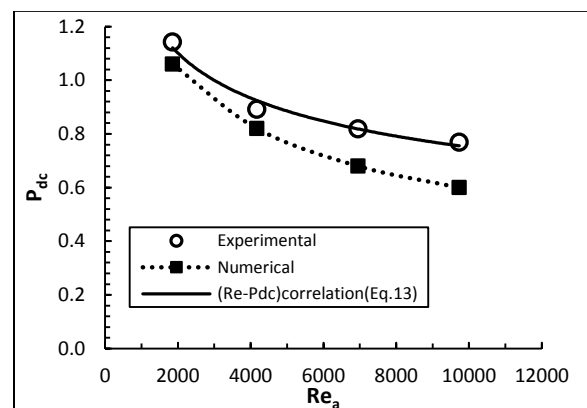
Fig. (13) Effect of Re_a on P_{dc} for the studied bundle

In this case, the effect of the viscosity is less important and the total drag is rather dominated by the inertia force.

4.4 Comparison of the Present Results with Others from Literature

Fig. (14) shows comparisons of the current proposed heat transfer correlation, Eq. (12) with others found in literatures.
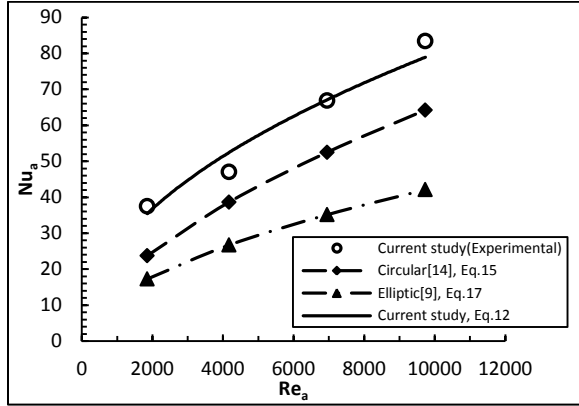
Fig. (14) Effect of Re_a on Nu_a for bundles with different tube shapes

Zukauskas [14] as referenced by Cengel, Y. A. [11] proposed a heat transfer correlation as following:

$$Nu_a = 0.35 \left(S_T \middle/ S_L \right)^{0.2} Re_a^{0.6} Pr_{af}^{0.36} \left(Pr_{af} \middle/ Pr_s \right)^{0.25} \quad \textbf{(14)}$$

$$(1000 \leq Re_a \leq 2 \times 10^5)$$

where, S_T and S_L are the transverse and longitudinal tube-pitches, respectively.
By applying a correction factor and other parameters form the present study, the above equation can be written as follows:

$$Nu_a = 0.2599 \, Re_a^{0.6} \quad (1000 \leq Re_a \leq 2 \times 10^5) \quad \textbf{(15)}$$

Ibrahim and Gomma [8] proposed a heat transfer correlation for elliptical tube bundle in cross flow of air in the following form:

$$Nu_a = 0.452 \, Re_a^{0.537} \, Pr_{af}^{0.33} \left(\frac{a}{b} \right)^{-0.079} (\sin(10+\alpha))^{0.2} \quad \textbf{(16)}$$

where, a and b are the minor and major axis of the elliptical tube, respectively. While, α is the flow angle of attack. To give the same surface area as wing-shaped tube of the current study, a and b are substituted by 0.0131 and 0.0301 m, respectively. By applying the current

experimental condition and using the D_{eq} to define Re_a, Eq. (16) can be reduced to:

$$Nu_a = 0.304 \, Re_a^{0.537} \quad (1500 \leq Re_a \leq 28000) \quad \textbf{(17)}$$

As seen in Fig. (14), for the given range of Re_a, the current bundle has increased values of Nu_a by about 34% and 70% comparing with those bundles with circular and elliptical tubes, respectively.

The correlation of pressure drop obtained from the present study is compared in Fig. (15), with the experimental correlation of Zukauskas [14], which is reduced as the following after introducing the current experimental condition and using the D_{eq} to define Re_a:

$$P_{dc} = 8.16 \, Re_a^{-0.207} \quad (1000 \leq Re_a \leq 20 \times 10^5) \quad \textbf{(18)}$$

Also, the comparison was conducted between the current results and those obtained by Ibrahim and Gomma [8], by applying the current experimental conditions and using the D_{eq} to define Re_a, the correlation is reduced to:

$$P_{dc} = 1.07 \, Re_a^{-0.047} \quad (1500 \leq Re_a \leq 28000) \quad \textbf{(19)}$$
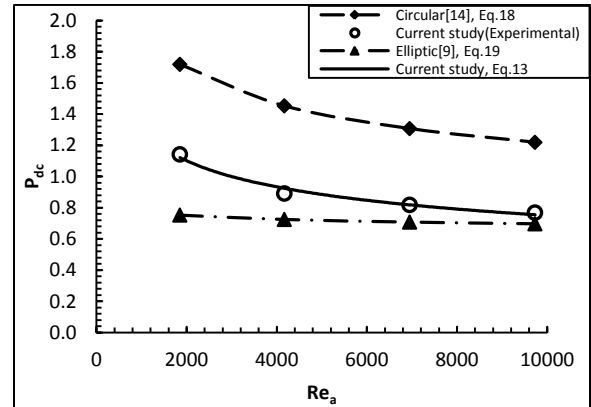
Fig. (15) Effect of Re_a on P_{dc} for the bundles with different tube shapes

It is also clear from Fig.(15), that the pressure drop coefficient of the bundle of wing-shaped tubes(P_{dc}) is significantly lower than that of the bundle with circular ones, by 37 % in average, and higher than that obtained for bundle with elliptical ones by 25 % in average. The low resistance to the flow that the bundle of wing-shaped tubes offers is attributed to the tubes layout. The streamlined shape of the wing-shaped tubes provides smaller frontal area than that of the circular tubes. This leads to a delay in the separation between the fluid boundary layer

and the surface of the tubes. It makes the separation point moves toward the rear stagnation point of the tubes. This makes the size of the weak region behind the tubes smaller and therefore less pressure drop is encountered.

4.5 Thermal Performance Criteria

Three methods are presented to resort a metric that expresses the global performance of the bundle of wing-shaped tubes heat exchanger with the particular reference of the traditional bundles with circular and elliptical tubes. These methods play as key design factors of the heat exchanger whilst incorporating an economic indicator, which are:

1. Direct comparison between the heat transfer coefficient (h_a) and the pressure drop (ΔP) at a fixed mass flow rate is conducted. This criterion allows quantifying the heat transfer enhancement for different tube bundle configurations with equivalent total pressure drops independently on the tube cross-sectional shape, Bergles et al.[15]

Fig. (16), shows the (h_a) versus the (P_{dc}) for different tube bundles under a constant mass flow rates. The maximum heat transfer coefficient (under the constraint of mass flow rates and a fixed pressure drop) is achieved when the tube bundle consists of wing-shaped tubes, while the worst performance is obtained when the bundle consists of elliptical tubes.
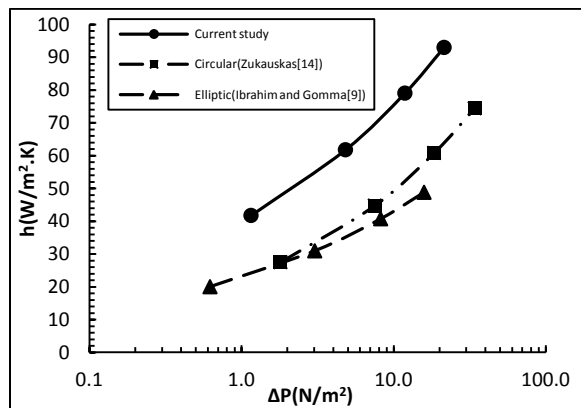
Fig. (16) Heat transfer coefficient versus pressure drop for bundle heat exchangers with different tube shapes

2. Scope of possible enhancement of the heat transfer per unit pumping power at a fixed mass flow rate, which is expressed by Eq. (20), Gomaa et al. [16].

$$\varepsilon = \frac{\rho_{af} \cdot c_{p_f} (T_{ai} - T_{ae})}{\Delta P_a} \qquad (20)$$

This criterion is more significant when the overall performance of the heat exchange surfaces is needed, while the cost of the heat transfer enhancement is in the same order of magnitude as the pumping power reduced.

Fig.(17) illustrates the effectiveness (ε) versus Re_a for bundles with wing-shaped, elliptical and circular tubes. It can, also, be seen that the bundle of wing-shaped tubes has the highest values of (ε).
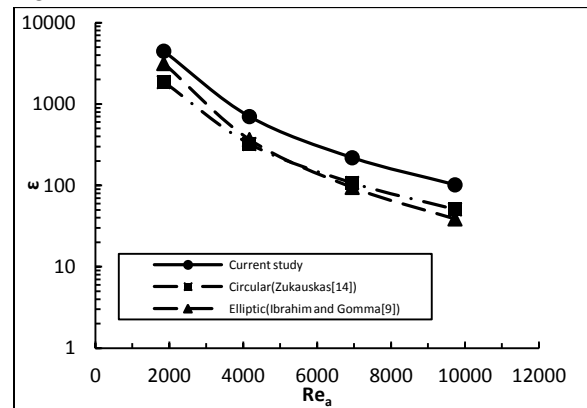
Fig. (17) Effectiveness ε versus Re_a for bundles with different tube shapes

3. The efficiency index (η) expresses the heat transfer performance (St) against the friction loss performance (P_{dc}) of the bundles with wing-shaped and elliptical tubes based on the bundle with circular ones performance, this definition was proposed by Afify et al. [17], as the following:

$$\eta = \frac{\left(St/St_c \right)}{\left(P_{dc}/P_{dc_c} \right)} \qquad (21)$$

The efficiency index (η) versus Re_a for bundles with wing-shaped and elliptical tubes is illustrated in Fig.(18)
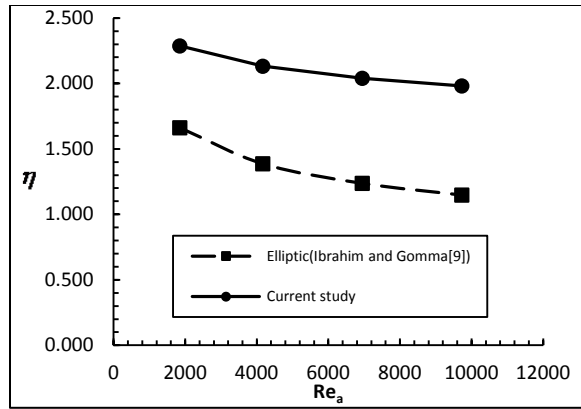
Fig. (18) Efficiency index η , versus Re_a for bundles with wing-shaped and elliptical tubes

It is evident that the bundle of wing-shaped tubes has the highest value of efficiency index comparing with the elliptical one.

Finally, the heat exchangers employing wing-shaped tubes arrangement contribute significantly to the energy conservation.

5. CONCLUSIONS

In current study the thermal and hydraulic performance of a bundle of staggered wing-shaped tubes undergoing cross-flow cooling has been studied experimentally and numerically for air side Re_a and water side Re_w. Based on the results of this study and the analysis of the impact of the controlling parameters, the following conclusions are proffered:

1. The study shows that, mainly the air flow Reynolds number, Re_a controls the heat transfer mechanism. It is found out that the effect of the water flow rate on the air flow heat transfer is insignificant. This is because of the high thermal resistance at the air side.

2. The heat transfer is correlated with (Re_a) and the results are shown in the dimensionless form of (Nu_a) as functions of (Re_a). The results indicate that Nu_a increases as Re_a increases in a power law relationship. For the bundle of wing-shaped tubes, the overall correlation are found as follows:

$$Nu_a = 0.94\,Re_a^{\,0.483}$$

$$1.85 \times 10^3 \leq Re_a \leq 9.7 \times 10^3$$

3. The air flow heat transfer results of the studied bundle are compared with those,

obtained from literature, which having different tubes shapes, with the same surface area and similar parameters as for the wing-shaped ones. The comparison revealed that utilizing the wing-shaped tubes minimizes the thermal resistance. The heat transfer enhancement in the case of using the bundle of wing-shaped tubes is higher than that obtained for those with circular and elliptical tubes by about 34% and 70%, respectively.

4. The variation of the non dimensional pressure drop coefficient (P_{dc}) for the air flow with Re_a is observed. It is found that P_{dc}, varies with Re_a in an inverse power law form. A pressure drop correlation for the bundle of wing-shaped tubes is proposed as:

$$P_{dc} = 6.731\,Re_a^{\,-0.238}$$

$$1.85 \times 10^3 \leq Re_a \leq 9.7 \times 10^3$$

5. It is revealed that by using the bundle of wing-shaped tubes, 37% reduction in the pressure drop as relative to that with circular ones is achieved. However, comparing with that of elliptical ones, 25% increasing in pressure drop is achieved.

6. Three methods (Direct comparison, effectiveness ε and the efficiency η index) are presented to resort a metric that expresses the thermal performance criteria of the bundle of wing-shaped tubes. The results indicate that, the bundle of wing-shaped tubes has the better performance over those with elliptical and circular ones for similar parameters and conditions.

Nomenclature

Alphabet- Upper Case

A_{so}	Total outer surface area of the tubes, m^2
D_{eq}	Equivalent circular diameter, m
Nu	Nusselt number, $(h.D_{eq})/k$
P_{dc}	Pressure drop coefficient, $(2.\Delta P_a)/(\rho_{af}.V_a^2)$
Pr	Prandtl number, $(\mu.c_p)/k$
Q	Heat transfer rate, W
R^2	coefficient of determination ranged from 0 to 1
Re	Reynolds number, $(\rho.V.D_{eq})/\mu$
St	Stanton number, $Nu/(R_e.Pr)$
T	Temperature, K
V	Velocity, m/s

Alphabet- lower Case

c_p	Specific heat at constant pressure, J/kg.K
h	heat transfer coefficient, $W/m^2.K$

178

k	thermal conductivity, W/m.K
m	Mass flow rate, kg/s
t	Tube thickness, m
x	Axial Coordinate
y	The normal distance to the tube surface
y^+	Dimensionless normal distance to the tube surface

Greek symbols

ε	Effectiveness, $(\rho_{af}.c_{pf}(T_{ai}-T_{ae}))/\Delta P_a$
μ	Absolute viscosity, Pa.s
η	Efficiency Index, $(St/St_c)/(P_{dc}/P_{dcc})$
ρ	Density, kg/m^3
α	Angle of attack, °
Δh_{dy}	Dynamic head difference, m H_2O
ΔT_{ln}	Log. mean temperature difference, K $(T_{ai}-T_{ae})/(ln(T_{ai}-T_s/T_{ae}-T_s))$
ΔP_a	Pressure drop across the bundle, Pa

Subscripts:

a	Air
c	circular
e	Exit
f	Film
i	Inlet
o	outer
w	Water

REFERENCES

[1] Zhukauskas, A., Ulinskas, R.V., [1985] " Efficiency parameters of heat transfer in tube banks", Heat Transfer Engineering, Vol.6, No.1, PP.19-25.

[2] Nada, S. A., El-Batsh, H., Moawed, M., [2007] " Heat transfer and fluid flow around semi-circular tube in cross flow at different orientations", International Journal of Heat Mass Transfer, Vol. 43, PP. 1157–1169.

[3] Brauer, H., [1964] " Compact heat exchangers", J. Chem. Process Eng, pp. 451-460.

[4] Horvat, A., Leskovar, M., Mavko, B., [2006] " Comparison of heat transfer conditions in tube bundle cross-flow for different tube shapes", International Journal of Heat and Mass Transfer, Vol. 49, pp. 1027-1038.

[5] Badr, H. M., [1998] " Forced convection from a straight elliptical tube", Heat and Mass Transfer , Vol. 34, pp. 229-236.

[6] Wilson, A. S., Bassiouny, M. K., [2000] " Modeling of heat transfer for flow across tube banks", Chemical Engineering Processing, Vol. 39, pp. 1-14.

[7] Nishiyama, H., Ota, T., Matsuno, T., [1988] " Heat transfer and flow around elliptic cylinders in tandem arrangement", JASME International Journal, Series II, Vol. 31, No. 3, pp. 410-419.

[8] Ibrahim, T. A., Gomma, A., [2009] " Thermal performance criteria of elliptic tube bundle in cross flow", International Journal of Thermal Sciences, Vol. 48, PP. 2148-2158.

[9] Ibrahiem, E.Z, Elsyed, A.O., Sayed Ahmed, ES., [2003] " Experimental investigation of the performance of a cross flow heat exchanger with bundle of semi-circular tubes", Mansoura Engineering Journal(MEJ), Vol.28, No.2.

[10] Ibrahiem, E.Z, Elsyed, A.O., Sayed Ahmed, ES., [2003] " Experimental study of air cooling and dehumidification around an in-line elliptic tubes bank in cross flow heat exchanger", The International Engineering conference (Mutah 2003), Mutah, Jordan.

[11] Cengel, Y.A., [1998] " Heat transfer a practical approach. McGraw- Hill, New Jersey.

[12] Holman, J.P., [2001] "Experimental methods for engineers", seventh ed. McGraw-Hill Int., New York, USA,.

[13]FLUENT 6.3.26 User's Guide, [2006], FLUENT Inc.

[14] Zukauskas, A., [1972] " Heat transfer from tubes in cross flow in Advances in Heat Transfer, Edited by Hartnett, J. P. and Irvine, T. F. Jr", New York: Academic Press. Vol. 8, pp. 93-160.

[15] Bergles, A., Blumenkra, A., Taborek, J., [1974] " Performance evaluation criteria for enhanced heat transfer surfaces", 4th Int. Heat Transfer Conference, Vol. 2, PP. 239–243.

[16] Gomaa, A., LeFeuvre, R., Underwood, C., Bond, T., [1999] " Numerical analysis of developing laminar flow and heat transfer characteristics through corrugated wall channels", IMechE 6th UK National Conference on Heat Transfer, UK, pp. 205–214.

[17] Afify, R., Berbish, N., Gomaa, A., Eid, A., [2004] " Numerical and experimental study of turbulent flow and convective heat transfer in a circular tube with disc-baffles", Engineering Research Journal 96, M37–M61, Faculty of Eng. at Mattaria, Egypt.